Hindawi Publishing Corporation
Mathematical Problems in Engineering
Volume 2008, Article ID 919420, 20 pages
doi:10.1155/2008/919420

Research Article

Peak Ground Acceleration Prediction by Artificial Neural Networks for Northwestern Turkey

Kemal Günaydın and Ayten Günaydın

Department of Civil Engineering, Eskişehir Osmangazi University, Batı Meşelik, 26480 Eskişehir, Turkey

Correspondence should be addressed to Kemal Günaydın, kgunaydi@ogu.edu.tr

Received 13 June 2008; Revised 5 September 2008; Accepted 12 October 2008

Recommended by Oleg Gendelman

Three different artificial neural network (ANN) methods, namely, feed-forward back-propagation (FFBP), radial basis function (RBF), and generalized regression neural networks (GRNNs) were applied to predict peak ground acceleration (PGA). Ninety five three-component records from 15 ground motions that occurred in Northwestern Turkey between 1999 and 2001 were used during the applications. The earthquake moment magnitude, hypocentral distance, focal depth, and site conditions were used as inputs to estimate PGA for vertical (U-D), east-west (E-W), and north-south (N-S) directions. The direction of the maximum PGA of the three components was also added to the input layer to obtain the maximum PGA. Testing stage results of three ANN methods indicated that the FFBPs were superior to the GRNN and the RBF for all directions. The PGA values obtained from the FFBP were modified by linear regression analysis. The results showed that these modifications increased the prediction performances.

1. Introduction

Knowing the characteristics of ground motions in a specified region is vital for the design of engineering structures. Peak ground acceleration (PGA) is commonly used to define the ground motions. Based on the historical ground motion records, several empirical equations were suggested through regression analysis for the estimation of PGA [1–7]. Different combinations of the earthquake characteristics and site condition were generally taken into consideration by the authors during the derivation of the equations. Douglas [8] performed an extensive analysis for earlier empirical formulas. As a result of this investigation very little agreement has been reached in the past 30 years of ground motion estimation relation studies since each formula had been derived based on the available data which varied greatly with geographical regions. The empirical attenuation relationships based on Turkish strong ground motion data were proposed by Aydan et al. [9], Inan et al. [10], Aydan [11], Gülkan and Kalkan [12], and Ulusay et al. [13].

Northwestern Turkey, which includes the Marmora region, is a densely populated and industrialized region of the country. In recent years, two destructive earthquakes Kocaeli (1999) (the moment magnitude, M_w = 7.4) and Düzce (1999) (M_w = 7.1) occurred in this area. As a result of comprehensive records from these ground motions, their aftershocks and other recent earthquakes, several investigations were performed to evaluate the PGA of this region. Some of these investigations were summarized as follows: Özbey [14] developed an attenuation relationship for peak horizontal acceleration using data from the Kocaeli (1999) and the Düzce (1999) earthquakes. Akyol et al. [15] evaluated attenuation and site effects of the 69 microearthquakes recorded at six stations located in different geological conditions in the city of Bursa, Marmora region, Turkey. Durukal [16] compared not only horizontal peak accelerations from the Kocaeli and Düzce earthquakes with the attenuation relationships derived by Boore et al. [3], Campbell [4], Sadigh et al. [5], and Atkinson and Boore [17] but also vertical peak accelerations from these earthquakes with the formulas of Campbell [4], and Atkinson and Boore [17]. From these comparisons, the author concluded that the attenuation relationships relied heavily on extrapolation from larger distances and smaller magnitude earthquakes to define ground motion predictions in the distance and magnitude range and could not yield correct values in the near field for large magnitude events. Fukushima et al. [18] investigated attenuation characteristics of PGA recorded on different sites during the Kocaeli (1999) and Düzce (1999) earthquakes and found that the PGA data of the Kocaeli earthquake showed good agreement with the attenuation relation derived by Fukushima and Tanaka [19]. Özbey et al. [20] used 195 recordings from 17 recent earthquakes including the Kocaeli (1999) and Düzce (1999) earthquakes and their aftershocks to develop empirical attenuation relationships of PGA and 5% damped spectral acceleration for Northwestern Turkey. Özel et al. [21] evaluated PGA values recorded on 19 different sites during the largest aftershock (M_w = 5.8) of the Kocaeli (1999) earthquake by using the empirical attenuation relationships derived by Fukushima and Tanaka [22] and Ansal [23].

Artificial neural networks (ANNs), however, are not defined as a specific equation form. They can infer solutions to problems having nonlinear and complex interaction among the variables and find functional relationship between the input and output of dataset. In recent years, considerable researches, some of which referenced in this paragraph, were performed to evaluate the PGA and response spectra of ground motions by using ANN methods. Dai and MacBeth [24, 25] used ANN to pick seismic arrivals from local earthquakes data. Dai and MacBeth [26] developed a back-propagation neural network to identify P- and S-arrivals from three-component recordings of local earthquake data. Giacinto et al. [27] applied the neural networks to evaluate earthquake risk for real geological structures. Ghaboussi and Lin [28] proposed a new method using the ANN to generate artificial earthquake accelerograms from response spectra. Lin and Ghaboussi [29] applied stochastic neural networks to generate multiple spectrum accelerograms from response spectra or design spectra. Kerh and Chu [30] estimated PGA at two main line sections of Kaohsiung Mass Rapid Transit in Taiwan by using three models of the FFBP structured different combination of epicentral distance, focal depth, and earthquake magnitude in the input layer and verified their results by using microtremor records. They also compared their results with those of available empirical formulas in the literature. Lee and Han [31] used five ANN-based models to generate artificial earthquake and response spectra. Baziar and Ghorbani [32] developed a neural network model to predict the horizontal ground displacement in both ground slope and free face conditions due to liquefaction-induced lateral spreading. Kerh and Ting [33] applied back-propagation neural networks obtained from different input combinations of epicentral distance, focal depth, and magnitude to predict PGA along

the high-speed rail system in Taiwan. Alves [34] used neural networks for earthquake forecasting. Barrile et al. [35] predicted seismic sequences of aftershocks occurred after a great earthquake by using radial basis function neural network. Liu et al. [36] evaluated the peak ground velocity for West America region. The authors used the earthquake magnitude, epicentre distance, site intensity, and site condition as inputs. As a result of this study, input parameters were ordered as earthquake magnitude, epicentral distance, and soil condition with respect to the importance of them on the peak ground velocity variations. Amiri and Bagheri [37] used wavelet multiresolution analysis and radial basis function neural network to generate artificial earthquake accelerograms from response spectrum.

The present study aimed at developing the PGA estimation models for Northwestern Turkey by using ANN methods. The PGA was modelled as function of earthquake moment magnitude (M_w), hypocentral distance (HD), focal depth (FD), and site conditions (SCs) for vertical, E-W and N-S directions, separately. The direction of the maximum PGA of the three components was also used as input to develop the maximum PGA model. Each model was calculated by using three different ANN methods such as FFBP, RBF, and GRNN. The result showed that the models of FFBP gave the best prediction performance under the conditions of used data. In order to improve prediction performance, the PGA values of FFBP were modified by the regression analysis.

2. Artificial neural network method

2.1. Feed-forward back-propagation networks

Feed-forward back-propagation (FFBP) networks have three components: an input layer, one or more hidden layers, and an output layer (see Figure 1). Each layer consists of one or more neurons (nodes). In the calculation process of problem solving, all input nodes are collected at each hidden node after being multiplied by weights. Later, a bias is attached to this sum, transformed through a nonlinearity function, and transferred to the next layer. There are several functions such as hyperbolic tangent, sigmoid and linear functions that can be used as transfer function. The same procedure can be followed in this layer to provide the network output results consequently. As the forward processing arrives at the output layer, the overall error between the network output and the actual observation is calculated. The error at the output layer propagates backward to the input layer through the hidden layer in the network to obtain the final desired outputs. During the forward pass all the synaptic weights of the networks are fixed. During the backward pass, on the other hand, all the synaptic weights are adjusted in accordance with an error-correction rule [38]. Figure 1 shows a typical FFBP structure used in this study. There are one input layer having x_n neurons, one hidden layer having h_m neurons, and one output layer having y_l neurons. Every node in the layer is connected with that in the next layer by interconnection strength, or weight (w). Input-to-hidden and hidden-to-output weights are named as w_{ij} and $w_{ik,}$ respectively. Mathematically the output of network (y_k) is computed by the equation

$$y_k = \tilde{f}\left[\sum_{j=1}^{m} w_{jk} \cdot f\left[\sum_{i=1}^{n}\left(w_{ij} \cdot x_i + b_1\right)\right] + b_2\right], \quad k = 1, 2, 3, \ldots, l, \tag{2.1}$$

where b_1 is the first layer bias, b_2 is the second layer bias, $f(\cdot)$ is activation function between input and hidden layers, and $\tilde{f}(\cdot)$ is activation function between hidden and output layers.

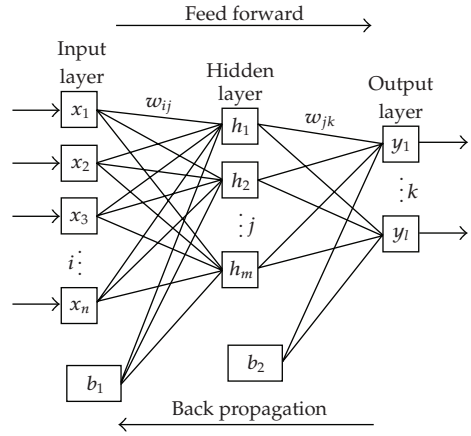

Figure 1: Schematic diagram of an FFBP.

The tangent sigmoid (tan-sigmoid), logarithmic sigmoid (log-sigmoid), and linear activation functions [38] are tried for both $f(\cdot)$ and $\tilde{f}(\cdot)$ to obtain the best prediction performance. The $f(\cdot)$ and $\tilde{f}(\cdot)$ types used in this study are presented in Section 4.

The back-propagation network (BPN) proposed by Rumelhart et al. [39] is used for learning model. The aim of this model is to minimize iteratively the global error or mean sum squared error (MSE), E, defined by

$$E = \frac{1}{2P}\sum_{p=1}^{P}\sum_{k=1}^{l}\left(T_{pk} - y_{pk}\right), \quad p = 1, 2, 3, \ldots, P, \tag{2.2}$$

where T_{pk} is the target (observed) output at kth output node of pth pattern, y_{pk} is the predicted output at kth output node of pth pattern, P is total number of training patterns. The global error (E) at the output layer propagates backward from the output to hidden layer in order to adjust the weights in each layer of the network during each iteration. The iterations are repeated until a specified convergence is reached or a given number of iterations are over.

Each step in the learning phase is called a Learning Epoch. In the present study Levenberg-Marquardt algorithm [40, 41] is used. It minimizes E while it tries to keep small the step between the old weights configuration (W_{old}) and the updated one (W_{new}). This algorithm can be written as follows:

$$W_{\text{new}} = W_{\text{old}} - \left[J^T J + \gamma I\right]^{-1} J^T E\left(W_{\text{old}}\right), \tag{2.3}$$

where J is the Jacobian of the error function E, I is the identity matrix, and γ is the parameter used to define the iteration step value [42]. The adaptive learning rate, which changes during the training stage dynamically, is used here. The learning rate takes values changing from 0 to 1. For each epoch, if performance decreases toward the goal, then the learning rate is increased by the factor learning increment. If performance increases, the learning rate is adjusted by the factor learning decrement. Throughout all FFBP simulations, the performance goal is taken as 0.00001. After the training phase of the network has been successfully

accomplished, performance of the trained model is tested with a different dataset. Details of the concept of FFBP networks and description of various training algorithms can be seen in Haykin [38], Bishop and Hinton [43], and Principe et al. [44].

The training input and output data of models are normalized by

$$x_{ni} = a \cdot \frac{x_i - x_{\min}}{x_{\max} - x_{\min}} + b, \tag{2.4}$$

where x_i is the observed data obtained from ith record, x_{n_i} is normalized value of ith record, $x_{\max}$ and $x_{\min}$ are the maximum and minimum values, respectively. Different values can be assigned for scaling factors a and b. There are no fixed rules as to which standardization approach should be used in particular circumstances [45, 46]. In this study, different a and b values were tried to obtain the best prediction performance, then, $a = 0.6$ and $b = 0.2$ were taken. Thus, both input and output data were normalized within the range 0.2–0.8. The relative better node numbers of the hidden layer were found by trial and error because there was no theory about the nodes numbers yet. The networks training were stopped after maximum 10000 epochs.

2.2. Radial basis function networks

Radial basis function (RBF) networks were introduced into the neural networks literature by Broomhead and Lowe [47]. The RBF consists of three layers, namely, input, hidden and output. It is a feed-forward network and has only one hidden layer (Figure 2). The input layer is made up of source nodes (sensory units) that connect the network to its environment. The second layer applies a nonlinear transformation from the input space to the hidden space; in most applications the hidden space is of high dimensionality. The output layer is linear, supplying the response of the network to the activation pattern (signal) applied to the input layer [38]. The input to each RBF neuron is treated as a measure of the difference between data and a "centre", which is a parameter of its transfer function (Figure 2). The transfer function of the neuron indicates the influence of data points at the centre. Generally this function is Gaussian and its centres can be chosen either randomly from the training data or they are iteratively trained or derived using techniques like K-means, Max-Min algorithms, Kohonen self organizing maps [38, 48]. After this unsupervised learning and cluster formations, the weights between the hidden and output layer neurons are determined by multiple regression in a supervised manner. The concept of such a fragmented learning is borrowed from certain biological neurons (doing, say, visual recognition), which function on the basis of "locally tuned response" to sensing. The RBF does not involve iterative training and hence much of the training time is saved [49]. The output y of an RBF is computed by the equation

$$y = f(x) = \sum_{i=1}^{m} w_i \cdot G\|x - c_i\| + w_o, \tag{2.5}$$

where m is number of hidden nodes ($i = 1, 2, 3, \ldots, m$), w_i is connection weights between the hidden neuron and output neuron, x is input feature vector, c is centre of the respective field, $\|x - c_i\|$ is the Euclidian distance between the prediction location (c_i), and each known data

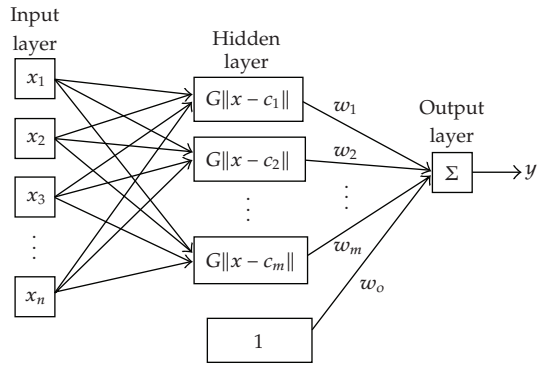

Figure 2: Schematic diagram of an RBF.

location (x) and $G\|x - c_i\|$ is radial basis function. The general class of radial basis function is Gaussian as given by (2.6):

$$G\|x - c_i\| = -\exp\left(-\sum_{i=1}^{m} \frac{\|x_i - c_i\|}{2\sigma_i^2}\right), \tag{2.6}$$

where σ_i is the width of the Gaussian function indicating selectivity of the neuron. In this study, the exact design RBF creating as many hidden neurons as there were input vectors was used [50]. Different spread constants were examined to find the best estimation performance of the RBF with zero error on training vectors.

2.3. Generalized regression neural networks

The generalized regression neural network (GRNN) was proposed by Specht [51] and reinvented by Schiøler and Hartmann [52]. The GRNN is Specht's term for Nadaraya-Watson kernel regression [53, 54]. It is based on established statistical principles and converges with an increasing number of samples asymptotically to the optimal regression surface [55].

Since the principle of the GRNN has been well documented in the literature [38, 51, 56], it is briefly explained in this section. As shown in Figure 3, the GRNN consists of four layers, including the input layer, pattern layer, summation layer, and output layer. Each input unit in the input layer corresponds to individual process parameter. The input layer is fully connected to the second, pattern layer, where each unit represents a training pattern and its output is a measure of the distance of the input from the stored patterns. Each pattern layer unit is connected to the two neurons in the summation layer: S- and D-summation neurons. The S-summation neuron computes the sum of the weighted outputs of the pattern layer while the D-summation neuron calculates the unweighted outputs of the pattern neurons. The connection weight between the ith neuron in the pattern layer and the S-summation neuron is y_i, the target output value corresponding to the ith input pattern. For D-summation neuron, the connection weight is unity. The output layer merely divides the output of each S-summation neuron by that of each D-summation neuron, yielding the

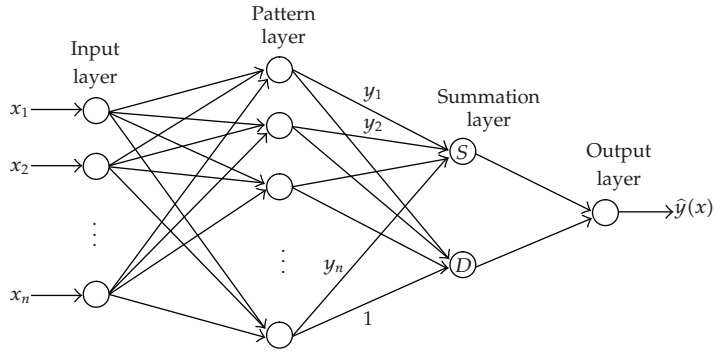

Figure 3: Schematic diagram of a GRNN.

predicted value to an unknown input vector x as

$$\hat{y}(x) = \frac{\sum_{i=1}^{n} y_i \exp\left[-D(x, x_i)\right]}{\sum_{i=1}^{n} \exp\left[-D(x, x_i)\right]}, \tag{2.7}$$

where n indicates the number of training patterns and the Gaussian D function in (2.7) is defined as

$$D(x, x_i) = \sum_{j=1}^{p} \left(\frac{x_j - x_{ij}}{\zeta} \right)^2, \tag{2.8}$$

where p indicates the number of elements of an input vector. The x_j and x_{ij} represent the jth element of x and x_i, respectively. The ζ is generally referred to as the spread, whose optimal value is experimentally determined. It should be noted that in conventional GRNN applications all units in the pattern layer have the same single spread [57]. The GRNN performance is controlled only by the spread factor during the training. In this study, different spreads were tried to obtain the best prediction performance.

3. Description of data

As presented in Table 1, fifteen ground motions that occurred at Northwestern region of Turkey between 1999-2000 were used in the ANN applications. Maps of study area were given in Figures 4(a) and 4(b). 95 PGA records resulting from the ground motions were downloaded from web sites of the Consortium of Organizations for Strong Motion Observation Systems (COSMOSs, 2008) for east-west (E-W), north-south (N-S), and Up-Down (U-D) directions. The records were determined from 11 accelerograph stations operated by Boğaziçi University's Kandilli Observatory and Earthquake Research Institute (see Table 2 and Figure 4(b)).

The local site conditions at an accelerograph station can affect the strong motion recorded. The widely accepted method of reflecting these effects is to classify the recording stations based on shear-velocity (V_s). But, information on V_s is currently lacking for most stations in Turkey. In order to categorize site conditions in Turkey some studies were

Table 1: Strong ground motions used for PGA estimations.

Earthquake	Date	Earthquake location		M_w	FD (km)	Record numbers
		Latitude (°N)	Longitude (°E)			
İzmit-Kocaeli	17.08.1999	40.7270	29.9900	7.4	15.00	10
Akyazi-Adapazarı	17.08.1999	40.6400	30.6500	5.5	15.30	1
Cinarcik-Yalova	19.08.1999	40.5900	29.0800	5.0	11.5	4
Hendek-Adapazari	22.08.1999	40.7400	30.6800	5.0	5.40	3
Hendek-Akyazi	23.08.2000	40.6800	30.1000	5.8	15.30	9
İzmit	31.08.1999	40.7500	29.9200	5.2	17.70	9
İzmit	13.09.1999	40.7700	30.1000	5.8	19.60	10
Marmara Sea	20.09.1999	40.6900	27.5800	5.0	16.40	10
Sapanca-Adapazarı	11.11.1999	40.7400	30.2700	5.7	22.00	10
Düzce	12.11.1999	40.7746	31.1870	7.1	10.00	10
Duzce Aftershock	12.11.1999	40.7500	31.1000	5.2	10.00	7
Duzce Aftershock	12.11.1999	40.7400	31.0500	5.4	10.00	7
Kaynaşlı-Bolu	12.11.1999	40.7500	31.3600	5.0	10.00	1
Hendek-Adapazari	27.11.1999	40.7100	30.7000	5.0	10.00	2
Northeast of Bolu	02.14.2000	40.9000	31.7500	5.0	15.70	2

Table 2: Recording stations used in this study.

Station no.	Station name	Latitude (°N)	Longitude (°E)
772	Yarimca Pektim, Yarimca	40.7639	29.7620
ARC	Arcelik, Darica	40.8236	29.3607
770	Heybeliada Hospital, Heybeliada	40.8688	29.0875
BUR	Tofas Factory, Bursa	40.2605	29.0680
769	Yapi-Kredi Plaza, Levent	41.0811	29.0111
777	Fatih Tomb, Fatih	41.0197	28.9500
779	Yesilkoy Airport, Yesilkoy	40.9822	28.8200
768	Nuclear Research Center, K. Cekmece	41.0237	28.7594
767	Ambarli Thermic Power Plant, Ambarli	40.9809	28.6926
766	Botas Gas Terminal, M. Ereglisi	40.9920	27.9796
DAR	Arslan Cimento Factory, Darica	40.7569	29.3673

performed by researchers, namely, Zaré and Bard [58], Gülkan and Kalkan [12], Ulusay et al. [13], and Özbey et al. [20]. In the present study, site conditions (SCs) given in the web site of COSMOS were used as rock, stiff, and soft. Since the SC was taken into consideration during the estimation of PGA some records lacking the SC in the web site were not downloaded.

The training of the networks was performed using 72 sets of data. Testing of networks was done using 23 datasets that were randomly selected among the whole data. As depicted in Figures 5(a) and 5(b), the M_w and FD values of test and train data varied in the range of 5.2 to 7.4 and 5.4 to 22 km, respectively. The HD values were given in the Figure 5(c). Figure 5(d) illustrated the site conditions of train and test data (selected as SC=1 for rock, SC=3 for stiff soil, and SC=5 for soft soil). The other numbers could also be selected for SC. As seen in this figure the site conditions were commonly soft and stiff soil types. Figures 5(e)–5(g) showed the PGA values for E-W, N-S, and U-D directions, respectively. The maximum PGA records of the three components were given in Figure 5(h).

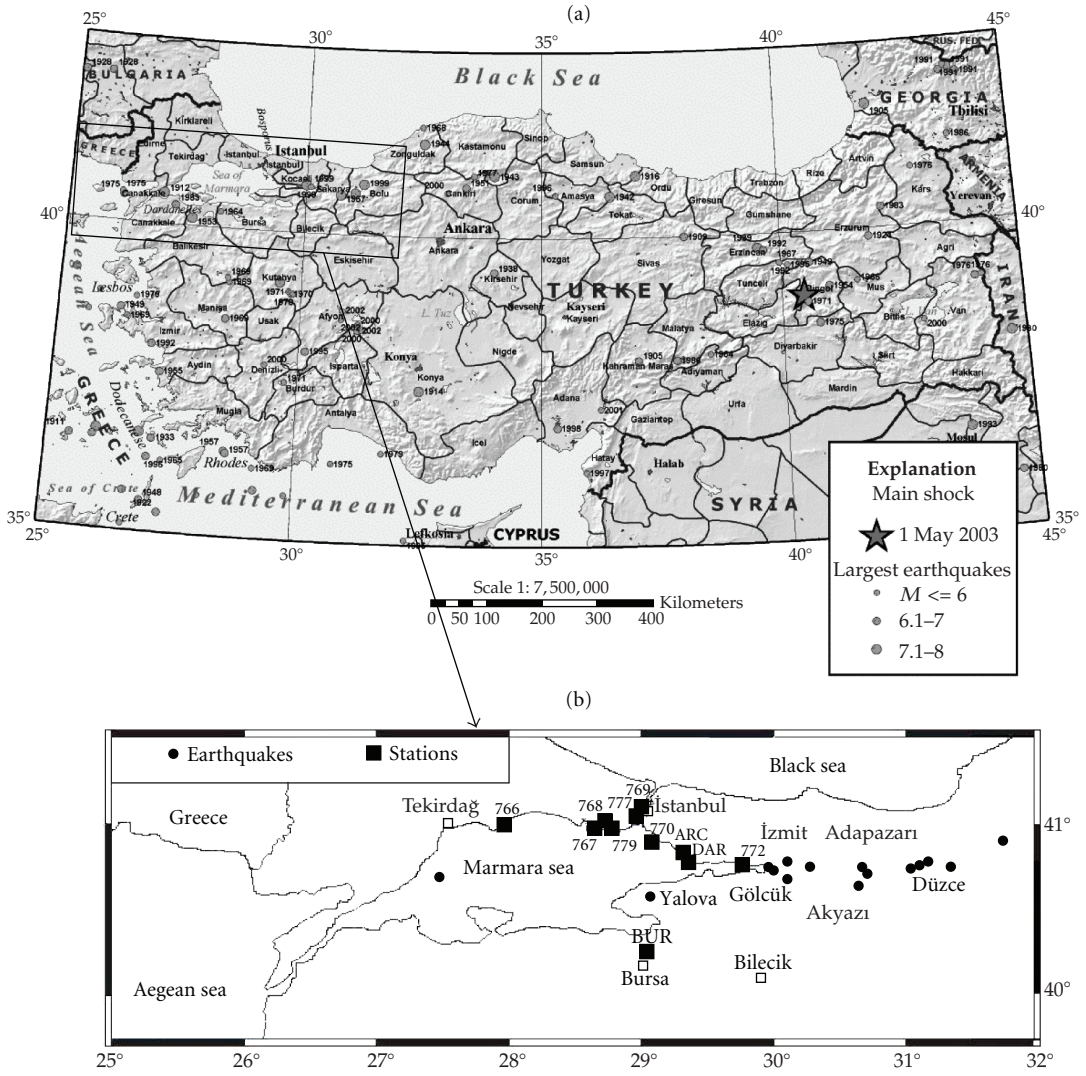

Figure 4: (a) Seismicity map of Turkey (http://neic.usgs.gov/). (b) Location map of the recording stations and earthquakes occurred in Northwestern Turkey.

4. Results and discussions

The PGA values were estimated by using three different ANN methods such as FFBP, RBF, and GRNN. Four models were developed for each ANN method. Models (i), (ii), and (iii) were used to determine the PGA values for E-W, N-S, and U-D directions, respectively. The input layer of these models consisted of four nodes representing the M_w, FD, HD, and SC values. The SC values in the models were used as 1, 3, and 5 for rock soil, stiff soil, and soft soil, respectively. Model (iv) was developed for estimation of maximum PGA values of the three components. The direction of maximum PGA (D) was varied for each record. Thus, the D (selected as D = 1 for E-W direction, D = 2 for N-S direction, and D = 3 for U-D direction) from a record was also used as input in this model. Inputs and outputs of each model were

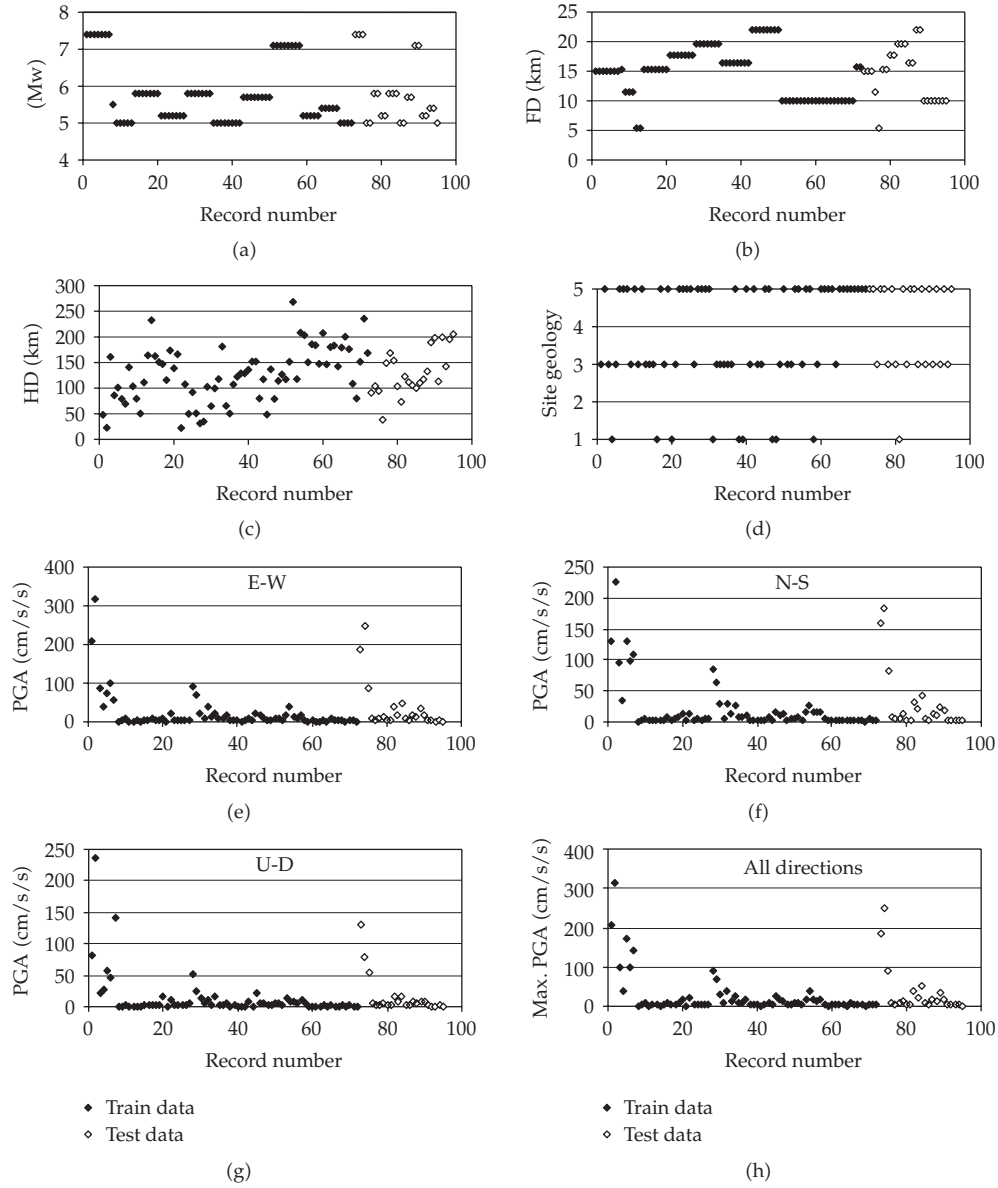

Figure 5: Record values of (a) M_w, (b) FD, (c) ED, (d) SC, (e) PGA for E-W direction, (f) PGA for N-S direction, (g) PGA for U-D direction, (h) maximum PGA of the three directions.

given in the second and third columns of Table 3, respectively. A program including MATLAB neural network toolbox was coded to train and test the models for each ANN method.

The models of the FFBP had one hidden layer in this paper. The node numbers of the hidden layer (h_m), the transfer function between input and hidden layers, $f(\cdot)$, and the transfer function between hidden and output layers, $\tilde{f}(\cdot)$, which gave the best testing performance, were presented in the forth, fifth, and sixth columns of Table 3, respectively. Similarly the spread values providing the most satisfactory testing performance for models of

Table 3: The final architectures of the models (i), (ii), (iii), (iv).

Model	Inputs	Outputs	FFBP method			GRNN method	RBF method
			h_m	$f(\cdot)$	$\tilde{f}(\cdot)$	Spread values	Spread values
(i)	M_w, FD, HD and SC	PGA for E-W	5	tan-sigmoid	log-sigmoid	0.015	0.022
(ii)	M_w, FD, HD and SC	PGA for N-S	5	log-sigmoid	log-sigmoid	0.062	0.039
(iii)	M_w, FD, HD and SC	PGA for U-D	2	tan-sigmoid	log-sigmoid	0.076	0.018
(iv)	M_w, FD, HD, SC and D	Max. PGA	7	log-sigmoid	log-sigmoid	0.28	0.060

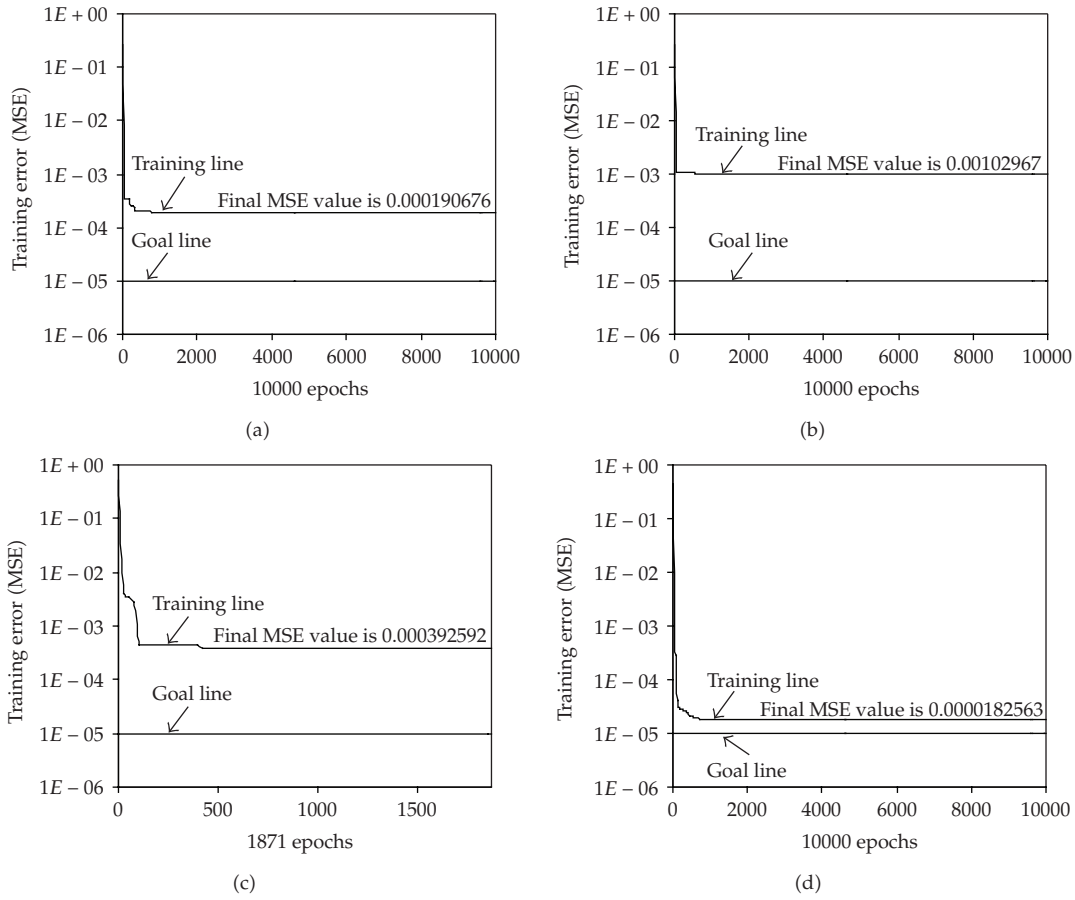

Figure 6: The training error graphs (a) for model (i), (b) for model (ii), (c) for model (iii) and (d) for model (iv).

the GRNN were given in the seventh column. Spread constants of the models for the RBF with zero error on training vectors were given in last column of Table 3. The training simulation performance of models of FFBP was evaluated in terms of the *MSE* values calculated from (2.2). The error graphs for models (i), (ii), (iii), and (iv) were presented in Figures 6(a), 6(b), 6(c), and 6(d), respectively. These figures showed that the networks had good convergence during the training data.

Table 4: *R*, *RMSE*, and *MAE* values of each ANN method for models (i), (ii), (iii), and (iv) in the test period.

Model	FFBP method			GRNN method			RBF method		
	R	*RMSE* (cm/s/s)	*MAE* (cm/s/s)	*R*	*RMSE* (cm/s/s)	*MAE* (cm/s/s)	*R*	*RMSE* (cm/s/s)	*MAE* (cm/s/s)
(i)	**0.998**	**5.52**	**4.06**	0.872	37.35	16.69	0.362	58.17	27.50
(ii)	**0.950**	**18.69**	**8.08**	0.891	22.91	10.22	0.481	43.61	16.99
(iii)	**0.999**	13.55	5.60	0.971	**8.10**	**2.85**	0.219	30.71	11.91
(iv)	**0.992**	**18.61**	**10.89**	0.895	41.57	17.79	0.550	50.48	27.21

The correlation coefficients (R), the root mean square error (*RMSE*), and the mean average error (*MAE*) used to evaluate the accuracy of each model are defined as

$$R = \frac{\sum_{i=1}^{n}(X_i - \overline{X}) - (Y_i - \overline{Y})}{\sqrt{\sum_{i=1}^{n}(X_i - \overline{X})^2 \cdot \sum_{i=1}^{n}(Y_i - \overline{Y})^2}}, \tag{4.1}$$

$$RMSE = \sqrt{\frac{1}{n}\sum_{i=1}^{n}(X_i - Y_i)^2}, \tag{4.2}$$

$$MAE = \frac{1}{n}\sum_{i=1}^{n}\left|X_i - Y_i\right|, \tag{4.3}$$

where X_i is observed *PGA* value at ith record, Y_i is predicted *PGA* value at ith record, n is total number of testing data, $\overline{X}$ and $\overline{Y}$ are the mean of X_i and Y_i, respectively.

The R measures the degree of linear association between the target and the realized outcome but the extreme values heavily affect it. The *RMSE* is specially suited for iterative algorithms and is a better measure for high values. The *MAE* has the advantage that it does not distinguish between the over- and underestimation and does not get too much influence by higher values [59, 60]. The *R*, *RMSE*, and *MAE* statistics of the models of each ANN in the test period were given in Table 4. According to the highest R and the smallest *RMSE* and *MAE* viewpoint, the models (i), (ii), and (iv) of FFBP showed the best performance. Although the R value of model (iii) of FFBP was the highest, the *RMSE* and *MAE* values of model (iii) of GRNN were the smallest.

The PGA estimates were plotted with observed values in the form of the time series and scatter plot. Figures 7(a, b), 7(c, d), 7(e, f), and 7(g, h) were drawn for models (i), (ii), (iii), and (iv), respectively. Figures 7(a) and 7(b) showed that the model of FFBP gave the best PGA prediction performance considering the highest correlation coefficient that was also given in the scatter plot, and the most agreements of the estimated with observed PGA values. The second best performance was provided from the GRNN. The RBF gave a quite poor performance. As illustrated in Figures 7(c) and 7(d), the results of RBF were the poorest. Although the results of FFBP and GRNN gave similar values for especially PGA < 50 cm/s/s, the estimation performance of FFBP ($R = 0.950$) for PGA > 50 cm/s/s was better than that of GRNN ($R = 0.891$). Figures 7(e) and 7(f) indicated that the FFBP and GRNN provided good prediction performances for PGA < 20 cm/s/s. The GRNN gave more satisfactory results than the FFBP for PGA > 20 cm/s/s while the correlation coefficient

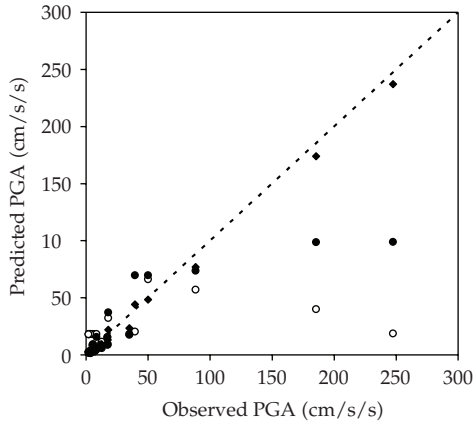
Predicted PGA (cm/s/s)
Observed PGA (cm/s/s)
0
50
100
150
200
250
300

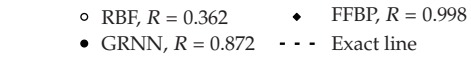
RBF, R = 0.362
FFBP, R = 0.998
GRNN, R = 0.872
Exact line

(a)

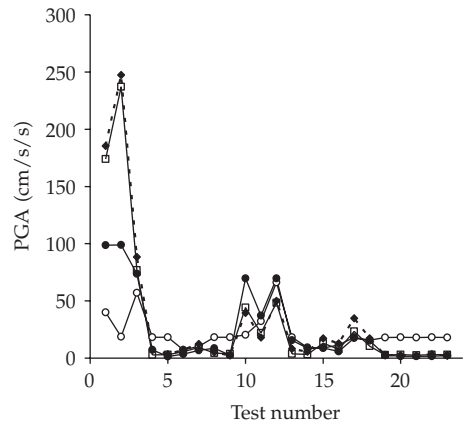
PGA (cm/s/s)
Test number
0
5
10
15
20
50
100
150
200
250
300


RBF
Observed
GRNN
FFBP

(b)

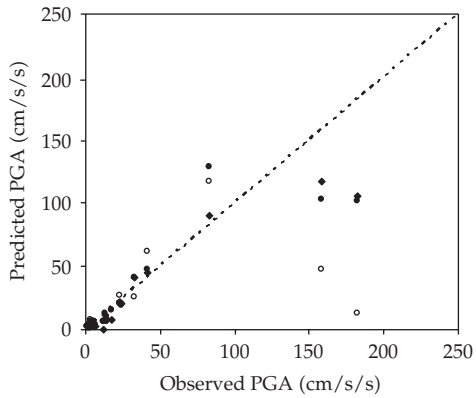
Predicted PGA (cm/s/s)
Observed PGA (cm/s/s)
0
50
100
150
200
250

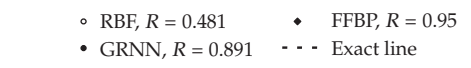
RBF, R = 0.481
FFBP, R = 0.95
GRNN, R = 0.891
Exact line

(c)

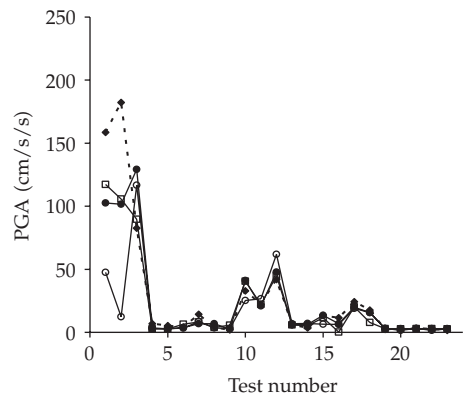
PGA (cm/s/s)
Test number
0
5
10
15
20
50
100
150
200
250


RBF
Observed
GRNN
FFBP

(d)

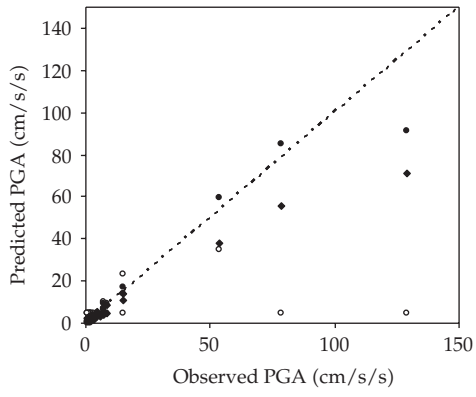
Predicted PGA (cm/s/s)
Observed PGA (cm/s/s)
0
20
40
60
80
100
120
140
150

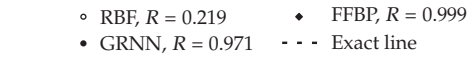
RBF, R = 0.219
FFBP, R = 0.999
GRNN, R = 0.971
Exact line

(e)

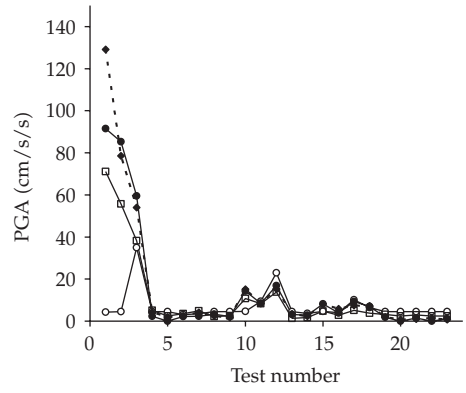
PGA (cm/s/s)
Test number
0
5
10
15
20
40
60
80
100
120
140


RBF
Observed
GRNN
FFBP

(f)

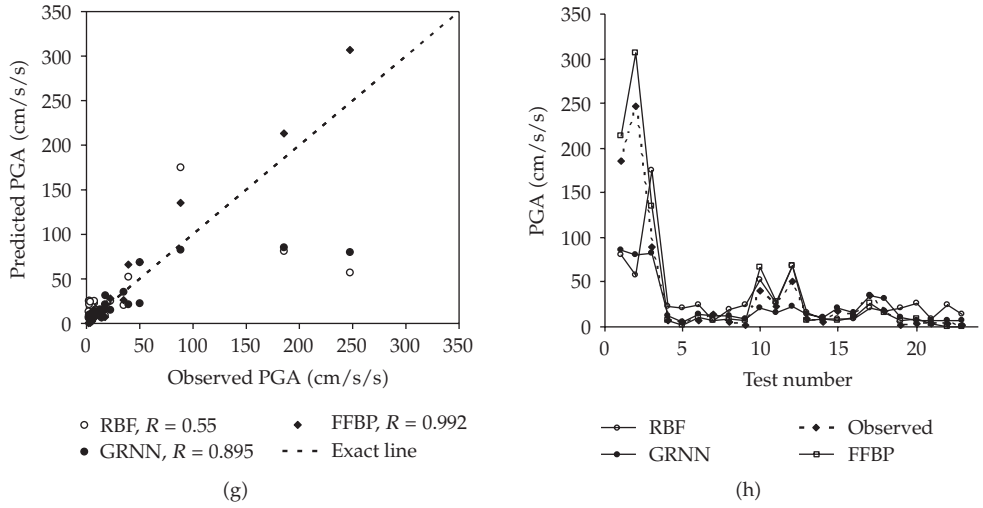

Figure 7: Observed and predicted PGA values (a, b) for E-W direction, (c, d) for N-S direction, (e, f) for U-D direction, (g, h) for maximum PGA direction in test period.

of FFBP results ($R = 0.999$) was superior to that of GRNN results ($R = 0.971$). The RBF predictions were unsatisfactory as seen from this figure. It was concluded from Figures 7(g) and 7(h) that the testing stage results determined by the FFBP method were more satisfactory than the other methods. The second best performance was provided by the GRNN. The performance of RBF ranked as the third.

The exact design RBF used in the applications is structured with zero training error on the design vectors hence it generates negative values for low PGA estimations. The GRNN, on the other hand, does not provide negative predictions. The GRNNs learn in one pass through the data and can generalize from samples as soon as they are stored. The FFBP requires an iterative training period differing from the RBF and GRNN.

Although the models of FFBP yielded considerably high correlation coefficients greater than 0.95, the predicted PGA values did not closely agree with observed PGA values except for E-W direction. A linear fit line was plotted for each model of FFBP in Figures 8(a), 8(c), 8(e), and 8(g). Therefore, some modifications were carried out as follows. We perform linear curve fitting of the form $y = a \cdot x + b$ to determine equations of these lines, that were given in (4.4)–(4.7), where y is predicted PGA value from the FFBP and x is observed PGA as follows:

$$y = 0.9518 \cdot x - 1.3243, \quad \text{for model (i)}, \tag{4.4}$$

$$y = 0.6839 \cdot x + 3.1888, \quad \text{for model (ii)}, \tag{4.5}$$

$$y = 0.5877 \cdot x + 1.8049, \quad \text{for model (iii)}, \tag{4.6}$$

$$y = 1.2346 \cdot x - 0.5589, \quad \text{for model (iv)}. \tag{4.7}$$

Equation of the exact lines in the scatter plots can be written as

$$y = x. \tag{4.8}$$

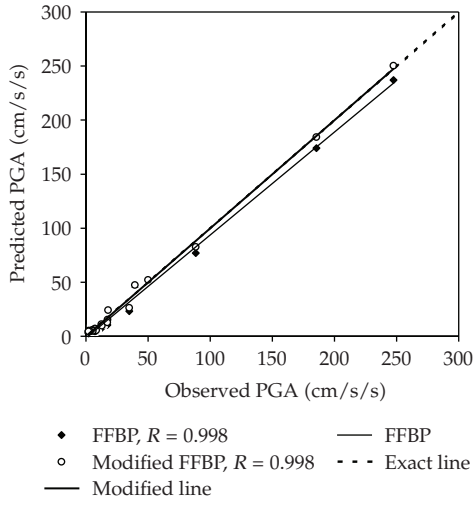

◆ FFBP, $R = 0.998$ —— FFBP
○ Modified FFBP, $R = 0.998$ - - - Exact line
—— Modified line

(a)

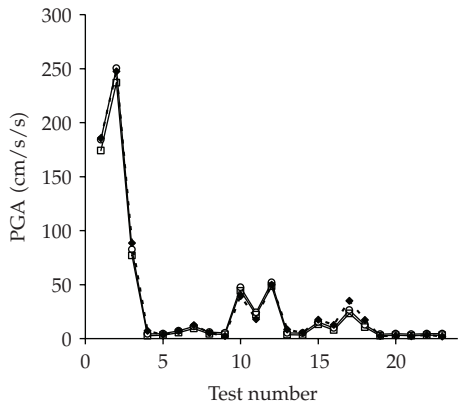

—○— Modified PGA by (4.9)
- - ◆ - - Observed PGA
—□— Predicted PGA by FFBP

(b)

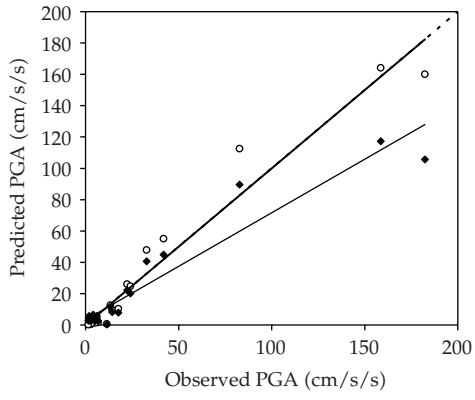

○ Modified FFBP, $R = 0.98$ —— FFBP
◆ FFBP, $R = 0.95$ - - - Exact line
—— Modified line

(c)

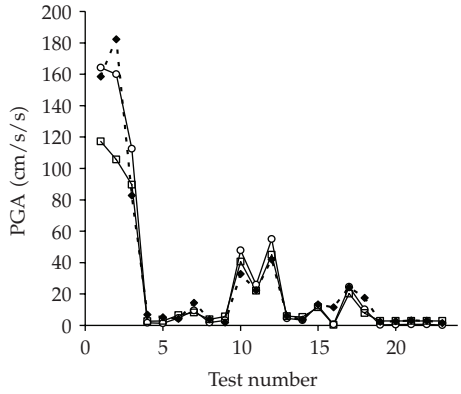

—○— Modified PGA by (4.10)
- - ◆ - - Observed PGA
—□— Predicted PGA by FFBP

(d)

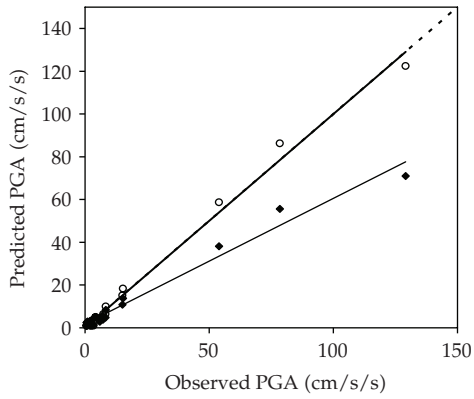

○ Modified ANN, $R = 0.996$ —— ANN
◆ ANN, $R = 0.999$ - - - Exact line
—— Modified ANN

(e)

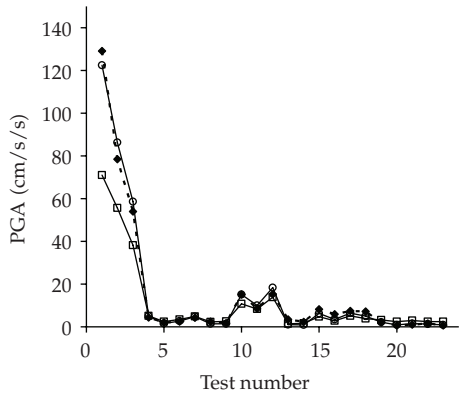

—○— Modified PGA by (4.11)
- - ◆ - - Observed PGA
—□— Predicted PGA by FFBP

(f)

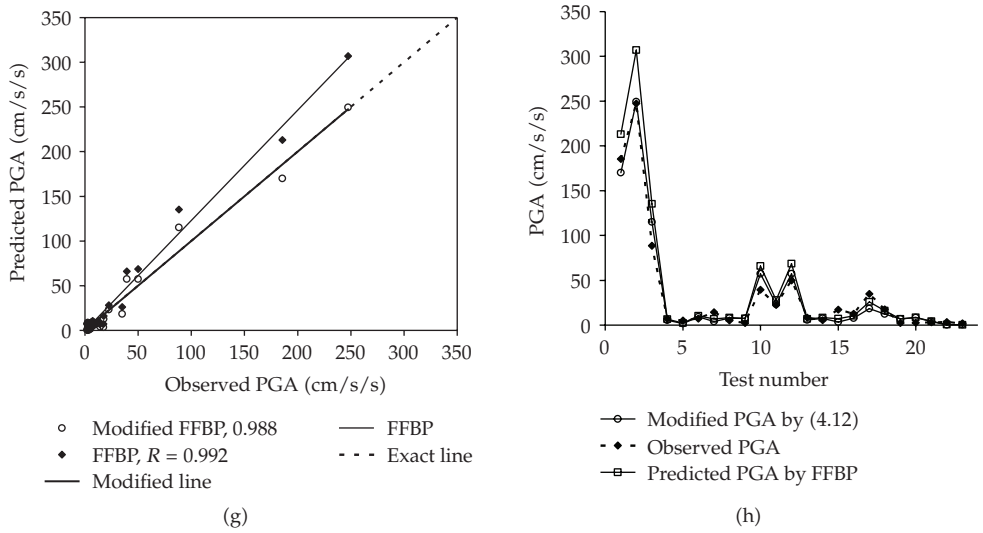

Figure 8: Comparison of FFBP and modified FFBP models and observed PGA values (a, b) for E-W direction, (c, d) for N-S direction, (e, f) for U-D direction, (g, h) for maximum PGA direction.

The predicted PGA values of models for the FFBP were modified by (4.9)–(4.12) to determine the same exact and fit lines as follows:

$$z = y + 0.0482 \cdot x + 1.3243, \quad \text{for model (i)}, \tag{4.9}$$

$$z = y + 0.3161 \cdot x - 3.1888, \quad \text{for model (ii)}, \tag{4.10}$$

$$z = y + 0.4123 \cdot x - 1.8049, \quad \text{for model (iii)}, \tag{4.11}$$

$$z = y - 0.2346 \cdot x + 0.5589, \quad \text{for model (iv)}, \tag{4.12}$$

where z is modified PGA values. As seen in scatter plots of each model, the fit lines plotted by using modified PGA values (z) were identical with exact lines. These lines were named as modified lines in the figures. The *R, RMSE,* and *MAE* statistics of modified models were given in Table 5. Good correlation was observed between the modified lines and modified PGA values ($R = 0.998$ for model (i), $R = 0.980$ for model (ii), $R = 0.996$ for model (iii), and $R = 0.988$ for model (iv)). The *RMSE* and *MARE* values of modified models (see Table 5) also showed better performance than those of models of FFBP (see Table 4) with these modifications and the PGA prediction performance of each model was considerably increased. The PGA values of model (i) of FFBP and modified model (i) were nearly identical with those of observed data (see Figures 8(a) and 8(b)(b)). As illustrated in Figures 8(c) and 8(d) the model (ii) gave good agreement with observed values except for the fist two test numbers. Although modified model (ii) gave more convenient results for high PGA values (PGA > 100 cm/s/s) than the model (ii) of FFBP, it gave a slightly poorer performance for small PGA values (PGA < 5 cm/s/s). Figure 8(e) showed that the model (iii) results of FFBP had similar trend with observed values while modified model (iii) results were fairly closed to observed values. It can be concluded from Figure 8(g) that modified model (iv) results provided better prediction performance than the model (iv) of FFBP.

Table 5: *R*, *RMSE*, and *MAE* values of modified models in the test period.

Model	*R*	*RMSE* (cm/s/s)	*MAE* (cm/s/s)
(i)	**0.998**	**3.64**	**2.86**
(ii)	**0.980**	**9.54**	**6.02**
(iii)	**0.996**	2.66	1.73
(iv)	**0.988**	**9.51**	**6.80**

Table 6: *R*, *RMSE*, and *MAE* values of each ANN method for models (v), (vi), (vii), (viii), and (ix) in the test period.

Model	Inputs	Outputs	FFBP method			GRNN method			RBF method		
			R	*RMSE* (cm/s/s)	*MAE* (cm/s/s)	*R*	*RMSE* (cm/s/s)	*MAE* (cm/s/s)	*R*	*RMSE* (cm/s/s)	*MAE* (cm/s/s)
(v)	M_w, FD and HD	PGA for E-W	**0.856**	**44.45**	**18.46**	0.829	46.89	18.63	0.487	55.68	29.79
(vi)	M_w, FD and HD	PGA for N-S	**0.122**	**33.22**	**16.43**	0.109	32.95	16.62	0.066	47.27	26.73
(vii)	M_w, FD and HD	PGA for U-D	0.093	98.38	93.61	**0.933**	**14.22**	**5.27**	0.751	21.87	10.16
(viii)	M_w, FD and HD	Max. PGA	**0.895**	**29.55**	**15.18**	0.882	45.29	19.38	0.563	61.52	37.75
(ix)	M_w, FD, HD and SC	Max. PGA	**0.667**	**46.27**	**21.94**	0.803	36.56	15.35	0.07	50.48	95.93

Models (v), (vi), (vii) of each ANN method were developed to show the effects of SC on the PGA prediction performance for E-W, N-S, and U-D directions, respectively. Models (viii) and (ix) were structured to check the SC and D effects on the maximum PGA prediction performance. The input variables of each model were given in the second column of Table 6. In order to compare these models with the models (i), (ii), (iii), and (iv), the same h_m, $f(\cdot)$ and $\tilde{f}(\cdot)$ for the models of FFBP, and the same spread values for the models of RBF and GRNN, which were given in Table 3, were used. The performance evaluation criteria (*R*, *RMSE*, and *MAE*) of models of each ANN method were given in Table 6. As seen in this table, the models (v), (vi), (vii), (viii), and (ix) gave a poorer prediction performance than the models (i), (ii), (iii), (iv) used the SC and D in the input layer (see Table 4) under the conditions of used ANN structures.

5. Conclusions

In this study, the PGA values were estimated for Northwestern Turkey by using three different ANN methods such as FFBP, RBF, and GRNN. The earthquake moment magnitude, epicentral distance, focal depth, and site conditions of strong motions were utilized as input parameters for predicting the PGA values for east-west, north-south, vertical directions. The direction of the maximum PGA of the three components was also added to the input layer to obtain the maximum PGA. The PGA values in each direction were calculated from each ANN method, separately. From these calculations, it was found that the model estimates of RBF were the poorest while those of FFBP were the best from the highest *R* and the smallest *RMSE* and *MAE* viewpoint. Although the GRNN gave considerably good performance for

PGA > 20 cm/s/s in vertical direction, it gave lower estimation performance than the FFBP for other directions and maximum PGA values.

Mathematical differences among the ANN methods can be briefly explained as follows. The RBFs generate negative values for low PGA estimations while the GRNN does not provide negative predictions. The GRNNs learn in one pass through the data and can generalize from samples as soon as they are stored. The FFBP has an iterative training period differing from the RBF and GRNN. Mathematical details can be found in Section 2.

Although the models of FFBP yielded high correlation coefficients (R) providing information for linear dependence between observations and corresponding estimations, the predicted PGA values were not fairly close to the observed values except for E-W direction. Thus, the predicted PGA values of FFBP were modified by linear regression analysis and more sensitive prediction performances were obtained.

This paper showed that the ANN methods could be applied successfully to derive the PGA models for Northwestern Turkey under used test and train data conditions. With further investigation, using more data from this region these models can be improved.

References

[1] W. B. Joyner and D. M. Boore, "Methods for regression analysis of strong-motion data," *Bulletin of the Seismological Society of America*, vol. 83, no. 2, pp. 469–487, 1993.

[2] N. N. Ambraseys, K. A. Simpson, and J. J. Bommer, "Prediction of horizontal response spectra in Europe," *Earthquake Engineering and Structural Dynamics*, vol. 25, no. 4, pp. 371–400, 1996.

[3] D. M. Boore, W. B. Joyner, and T. E. Fumal, "Equations for estimating horizontal response spectra and peak acceleration from western North American earthquakes: a summary of recent work," *Seismological Research Letters*, vol. 68, no. 1, pp. 128–153, 1997.

[4] K. W. Campbell, "Empirical near-source attenuation relationships for horizontal and vertical components of peak ground acceleration, peak ground velocity, and pseudo-absolute acceleration response spectra," *Seismological Research Letters*, vol. 68, no. 1, pp. 154–179, 1997.

[5] K. Sadigh, C.-Y. Chang, J. A. Egan, F. Makdisi, and R. R. Youngs, "Attenuation relationships for shallow crustal earthquakes based on California strong motion data," *Seismological Research Letters*, vol. 68, no. 1, pp. 180–189, 1997.

[6] P. Spudich, J. B. Fletcher, M. Hellweg, et al., "SEA96—a new predictive relation for earthquake ground motions in extensional tectonic regimes," *Seismological Research Letters*, vol. 68, no. 1, pp. 190–198, 1997.

[7] G. M. Atkinson and D. M. Boore, "Earthquake ground-motion prediction equations for eastern North America," *Bulletin of the Seismological Society of America*, vol. 96, no. 6, pp. 2181–2205, 2006.

[8] J. Douglas, "Earthquake ground motion estimation using strong-motion records: a review of equations for the estimation of peak ground acceleration and response spectral ordinates," *Earth-Science Reviews*, vol. 61, no. 1-2, pp. 43–104, 2003.

[9] Ö. Aydan, M. Sezaki, and R. Yarar, "The seismic characteristics of Turkish earthquakes," in *Proceedings of the 11th World Conference on Earthquake Engineering*, Acapulco, Mexico, June 1996, CD Paper no. 1025.

[10] E. Inan, Z. Colakoglu, N. Koc, N. Bayülke, and E. Coruh, *Earthquake Catalogs with Acceleration Records from 1976 to 1996*, General Directorate of Disaster Affairs, Earthquake Research Department, Ankara, Turkey, 1996.

[11] Ö. Aydan, "Comparison of suitability of submerged tunnel and shield tunnel for subsea passage of Bosphorus," *Geological Engineering Journal of Turkey*, vol. 25, no. 1, pp. 1–17, 2001 (Turkish).

[12] P. Gülkan and E. Kalkan, "Attenuation modeling of recent earthquakes in Turkey," *Journal of Seismology*, vol. 6, no. 3, pp. 397–409, 2002.

[13] R. Ulusay, E. Tuncay, H. Sonmez, and C. Gokceoglu, "An attenuation relationship based on Turkish strong motion data and iso-acceleration map of Turkey," *Engineering Geology*, vol. 74, no. 3-4, pp. 265–291, 2004.

[14] C. Özbey, *Empirical peak horizontal acceleration relationship for northwestern Turkey*, M.S. thesis, Boğaziçi University, Istanbul, Turkey, 2001.

[15] N. Akyol, A. Akinci, and H. Eyidogan, "Separation of source, propagation and site effects from S waves of local earthquakes in Bursa Region, Northwestern Turkey," *Pure and Applied Geophysics*, vol. 159, no. 6, pp. 1253–1269, 2002.

[16] E. Durukal, "Critical evaluation of strong motion in Kocaeli and Düzce (Turkey) earthquakes," *Soil Dynamics and Earthquake Engineering*, vol. 22, no. 7, pp. 589–609, 2002.
[17] G. M. Atkinson and D. M. Boore, "Some comparisons between recent ground-motion relations," *Seismological Research Letters*, vol. 68, no. 1, pp. 24–40, 1997.
[18] Y. Fukushima, O. Köse, T. Yürür, P. Volant, E. Cushing, and R. Guillande, "Attenuation characteristics of peak ground acceleration from fault trace of the 1999 Kocaeli (Turkey) earthquake and comparison of spectral acceleration with seismic design code," *Journal of Seismology*, vol. 6, no. 3, pp. 379–396, 2002.
[19] Y. Fukushima and T. Tanaka, "Revised attenuation relation of peak horizontal acceleration by using a new data base," Programme and Abstracts, SSJ 2, 116, 1992.
[20] C. Özbey, A. Sari, L. Manuel, M. Erdik, and Y. Fahjan, "An empirical attenuation relationship for Northwestern Turkey ground motion using a random effects approach," *Soil Dynamics and Earthquake Engineering*, vol. 24, no. 2, pp. 115–125, 2004.
[21] N. M. Özel, T. Sasatani, and O. Özel, "Strong ground motion during the largest aftershock (M_w = 5.8) of the 1999 Izmit earthquake, Turkey," *Tectonophysics*, vol. 391, no. 1–4, pp. 347–355, 2004.
[22] Y. Fukushima and T. Tanaka, "A new attenuation relation for peak horizontal acceleration of strong earthquake ground motion in Japan," *Bulletin of the Seismological Society of America*, vol. 80, no. 4, pp. 757–783, 1990.
[23] A. M. Ansal, "Istanbul için tasarim deprem özelliklerinin belirlenmesi," in *Proceedings of Prof. Dr. Rifat Yarar Symposium*, vol. 1, pp. 233–244, Istanbul, Turkey, December 1997.
[24] H. Dai and C. Macbeth, "Automatic picking of seismic arrivals in local earthquake data using an artificial neural network," *Geophysical Journal International*, vol. 120, no. 3, pp. 758–774, 1995.
[25] H. Dai and C. MacBeth, "The application of back-propagation neural network to automatic picking seismic arrivals from single-component recordings," *Journal of Geophysical Research B*, vol. 102, no. B7, pp. 15105–15113, 1997.
[26] H. Dai and C. MacBeth, "Application of back-propagation neural networks to identification of seismic arrival types," *Physics of the Earth and Planetary Interiors*, vol. 101, no. 3-4, pp. 177–188, 1997.
[27] G. Giacinto, R. Paolucci, and F. Roli, "Application of neural networks and statistical pattern recognition algorithms to earthquake risk evaluation," *Pattern Recognition Letters*, vol. 18, no. 11–13, pp. 1353–1362, 1997.
[28] J. Ghaboussi and C.-C. J. Lin, "New method of generating spectrum compatible accelerograms using neural networks," *Earthquake Engineering and Structural Dynamics*, vol. 27, no. 4, pp. 377–396, 1998.
[29] C.-C. J. Lin and J. Ghaboussi, "Generating multiple spectrum compatible accelerograms using stochastic neural networks," *Earthquake Engineering and Structural Dynamics*, vol. 30, no. 7, pp. 1021–1042, 2001.
[30] T. Kerh and D. Chu, "Neural networks approach and microtremor measurements in estimating peak ground acceleration due to strong motion," *Advances in Engineering Software*, vol. 33, no. 11-12, pp. 733–742, 2002.
[31] S. C. Lee and S. W. Han, "Neural-network-based models for generating artificial earthquakes and response spectra," *Computers and Structures*, vol. 80, no. 20-21, pp. 1627–1638, 2002.
[32] M. H. Baziar and A. Ghorbani, "Evaluation of lateral spreading using artificial neural networks," *Soil Dynamics and Earthquake Engineering*, vol. 25, no. 1, pp. 1–9, 2005.
[33] T. Kerh and S. B. Ting, "Neural network estimation of ground peak acceleration at stations along Taiwan high-speed rail system," *Engineering Applications of Artificial Intelligence*, vol. 18, no. 7, pp. 857–866, 2005.
[34] E. I. Alves, "Earthquake forecasting using neural networks: results and future work," *Nonlinear Dynamics*, vol. 44, no. 1–4, pp. 341–349, 2006.
[35] V. Barrile, M. Cacciola, S. D'Amico, A. Greco, F. C. Morabito, and F. Parrillo, "Radial basis function neural networks to foresee aftershocks in seismic sequences related to large earthquakes," in *Proceedings of the 13th International Conference on Neural Information Processing, Part II (ICONIP '06)*, vol. 4233 of *Lecture Notes in Computer Science*, pp. 909–916, Hong Kong, October 2006.
[36] B.-Y. Liu, L.-Y. Ye, M.-L. Xiao, and S. Miao, "Peak ground velocity evaluation by artificial neural network for west America region," in *Proceedings of the 13th International Conference on Neural Information Processing, Part II (ICONIP '06)*, vol. 4233 of *Lecture Notes in Computer Science*, pp. 942–951, Hong Kong, October 2006.
[37] G. G. Amiri and A. Bagheri, "Application of wavelet multiresolution analysis and artificial intelligence for generation of artificial earthquake accelerograms," *Structural Engineering and Mechanics*, vol. 28, no. 2, pp. 153–166, 2008.

[38] S. Haykin, *Neural Networks: A Comprehensive Foundation*, Prentice-Hall, Englewood Cliffs, NJ, USA, 2nd edition, 1999.
[39] D. E. Rumelhart, G. E. Hinton, and R. J. Williams, "Learning internal representation by error backpropagation," in *Parallel Distributed Processing: Explorations Microstructure of Cognition*, vol. 1, pp. 318–362, MIT Press, Cambridge, Mass, USA, 1986.
[40] K. Levenberg, "A method for the solution of certain non-linear problems in least squares," *Quarterly of Applied Mathematics*, vol. 2, pp. 164–168, 1944.
[41] D. Marquardt, "An algorithm for least-squares estimation of nonlinear parameters," *Journal of the Society for Industrial & Applied Mathematics*, vol. 11, pp. 431–441, 1963.
[42] A. Panizzo and R. Briganti, "Analysis of wave transmission behind low-crested breakwaters using neural networks," *Coastal Engineering*, vol. 54, no. 9, pp. 643–656, 2007.
[43] C. M. Bishop and G. Hinton, *Neural Networks for Pattern Recognition*, Clarendon Press, Oxford, UK, 1995.
[44] J. C. Principe, N. R. Euliano, and W. C. Lefebvre, *Neural and Adaptive Systems: Fundamentals through Simulation*, John Wiley & Sons, New York, NY, USA, 1999.
[45] F. Altun, Ö. Kişi, and K. Aydin, "Predicting the compressive strength of steel fiber added lightweight concrete using neural network," *Computational Materials Science*, vol. 42, no. 2, pp. 259–265, 2008.
[46] C. W. Dawson and R. Wilby, "An artificial neural network approach to rainfall-runoff modelling," *Hydrological Sciences Journal*, vol. 43, no. 1, pp. 47–66, 1998.
[47] D. Broomhead and D. Lowe, "Multivariable functional interpolation and adaptive networks," *Complex Systems*, vol. 2, no. 3, pp. 321–355, 1988.
[48] T. Kohonen, *Self-Organizing Maps*, Springer, Berlin, Germany, 2nd edition, 1997.
[49] R. Kalra and M. C. Deo, "Derivation of coastal wind and wave parameters from offshore measurements of TOPEX satellite using ANN," *Coastal Engineering*, vol. 54, no. 3, pp. 187–196, 2007.
[50] H. Demuth, M. Beale, and M. Hagan, *Neural Network Toolbox: For Use with Matlab*, Mathworks, Natick, Mass, USA, 2006.
[51] D. F. Specht, "A general regression neural network," *IEEE Transactions on Neural Networks*, vol. 2, no. 6, pp. 568–576, 1991.
[52] H. Schiøler and U. Hartmann, "Mapping neural network derived from the Parzen window estimator," *Neural Networks*, vol. 5, no. 6, pp. 903–909, 1992.
[53] E. A. Nadaraya, "On estimating regression," *Theory of Probability and Its Applications*, vol. 9, no. 1, pp. 141–142, 1964.
[54] G. S. Watson, "Smooth regression analysis," *Sankhyā, Series A*, vol. 26, part 4, pp. 359–372, 1964.
[55] D. Tomandl and A. Schober, "A Modified General Regression Neural Network (MGRNN) with new, efficient training algorithms as a robust 'black box'-tool for data analysis," *Neural Networks*, vol. 14, no. 8, pp. 1023–1034, 2001.
[56] L. H. Tsoukalas and R. E. Uhrig, *Fuzzy and Neural Approached in Engineering*, John Wiley & Sons, New York, NY, USA, 1997.
[57] B. Kim, D. W. Lee, K. Y. Park, S. R. Choi, and S. Choi, "Prediction of plasma etching using a randomized generalized regression neural network," *Vacuum*, vol. 76, no. 1, pp. 37–43, 2004.
[58] M. Zaré and P.-Y. Bard, "Strong motion dataset of Turkey: data processing and site classification," *Soil Dynamics and Earthquake Engineering*, vol. 22, no. 8, pp. 703–718, 2002.
[59] R. Kalra, M. C. Deo, R. Kumar, and V. K. Agarwal, "RBF network for spatial mapping of wave heights," *Marine Structures*, vol. 18, no. 3, pp. 289–300, 2005.
[60] N. Karunanithi, W. J. Grenney, D. Whitley, and K. Bovee, "Neural networks for river flow prediction," *Journal of Computing in Civil Engineering*, vol. 8, no. 2, pp. 201–220, 1994.